Nuclear Instruments and Methods in Physics Research A236 (1985) 274–283
North-Holland, Amsterdam

TEST OF A RING IMAGING CHERENKOV COUNTER

D. DRESSELHAUS and R. FOHRMANN *

*II. Institut für Experimentalphysik der Universität Hamburg **, Hamburg, Fed. Rep. Germany*

Received 22 November 1984

We have tested a ring imaging Cherenkov counter with readout of the projection chamber type. A specific detector response of $N_0 = 80\ \mathrm{cm}^{-1}$ was measured which corresponds to 8 photoelectrons per event in 1.60 m long nitrogen radiator. The resolution of the ring radius was measured to be $\Delta r/r = 3.6\%$. The crosstalk between neighboring wires due to photons generated in the avalanche process was estimated to contribute up to 50% per hit. It was reduced considerably by inserting shielding walls between the wires and by adding C_2H_6 or iC_4H_{10} to the CH_4–TMAE gas mixture.

1. Introduction

The Cherenkov radiation emitted by a fast charged particle traversing a radiator lies on a circular cone coaxial with the particle trajectory. The opening angle Θ of the cone is given by

$$\cos\Theta = \frac{1}{\beta n}, \tag{1}$$

where β is the particle velocity and n the index of refraction of the radiator. It was first proposed by Roberts to collect the Cherenkov light by a telescope objective [1]. Séguinot and Ypsilantis used photosensitive gases in a multiwire proportional chamber as a photon detector [2]. In such a set-up the light of the cone is focussed by a lens or a mirror to a ring image in the focal plane. The radius of the ring is given by

$$r = f\tan\Theta, \tag{2}$$

where f is the focal length of the mirror. Fig. 1 shows the schematic of a ring imaging counter. The photon detector is placed in the focal plane at a distance of $f = R/2$, where R is the radius of the spherical mirror. The photoelectron yield is

$$N_{\mathrm{pe}} = N_0 L \sin^2\Theta, \tag{3}$$

where L is the radiator length and N_0 is a constant which characterizes the quality of the detector:

$$N_0 = 370[\mathrm{eV}^{-1}\,\mathrm{cm}^{-1}]\int \eta Q R T \mathrm{d}E; \tag{4}$$

η is the electron detection efficiency, Q is the quantum efficiency for photon conversion, R is the mirror reflectivity and T is the transmission of the several detector components involved (radiator gas, windows, drift gas, and field shaping wires). For good Cherenkov counters with photomultipliers N_0 is on the order of 100 cm^{-1}. Among the various method for photon detection two different devices have turned out to be the most promising, the multistep chamber, which is already in use for experiment E605 at Fermilab [3] and the time projection chamber [4]. This paper reports on the measurements with a test set-up of the latter type.

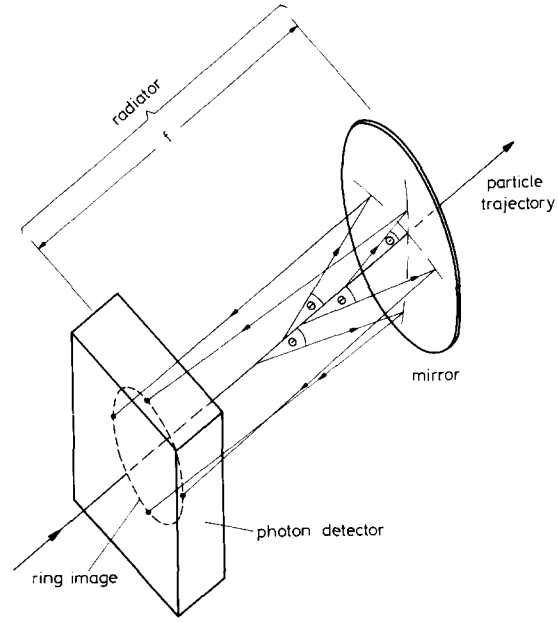

Fig. 1. Schematic view of a ring imaging Cherenkov counter.

* Now at Deutsches Elektronen-Synchrotron DESY, Hamburg, FRG.

** Supported by the Deutsches Bundesministerium für Forschung und Technologie.

2. The photon detector

Fig. 2 illustrates the basic idea of the photon detector. The Cherenkov photons enter the chamber through an entrance window with a suitable transmission to match the region of photoionization of the photosensitive gas. A photon is converted to an electron via

$$\gamma + M \rightarrow M^{+} e^{-},$$

where M is a molecule of the photosensitive gas. The conversion points of the Cherenkov photons lie on a circle which is read out two-dimensionally by drifting the electrons to the multiwire proportional chamber at the bottom of the detector. The x coordinate of the conversion point is given by the corresponding wire position, the y coordinate by the electron drift time: $y = v_d t$, assuming a uniform electric field in the drift region.

The choice of the geometry of the detector components and their physical properties were guided by the possible use of such a ring imaging detector in a high energy physics experiment. For the drift gas methane was chosen because it has a high drift velocity of 10 cm/μs and a low diffusion coefficient $\sigma = 250$ μm/cm$^{1/2}$. The multiwire proportional chamber is equipped with 40 goldplated tungsten wires with diameters of 20 μm which are 2.5 mm apart. The gap between the anode wires and the cathode is 4 mm. Each wire is connected to a low noise transimpedance amplifier (LeCroy TRA 403) with a gain of 50 mV/μA and a noise of 50 nA. The output signal is fed through a discriminator and a line receiver into a TDC unit (LeCroy 2770A) which is set to 10 ns per channel.

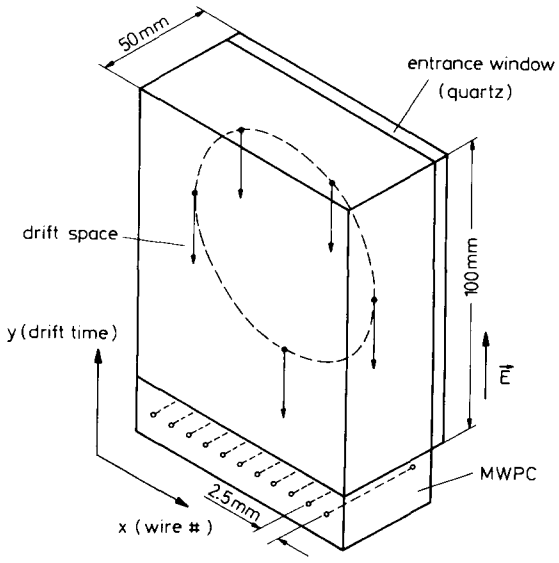

Fig. 2. Time projection chamber readout of the Cherenkov ring image.

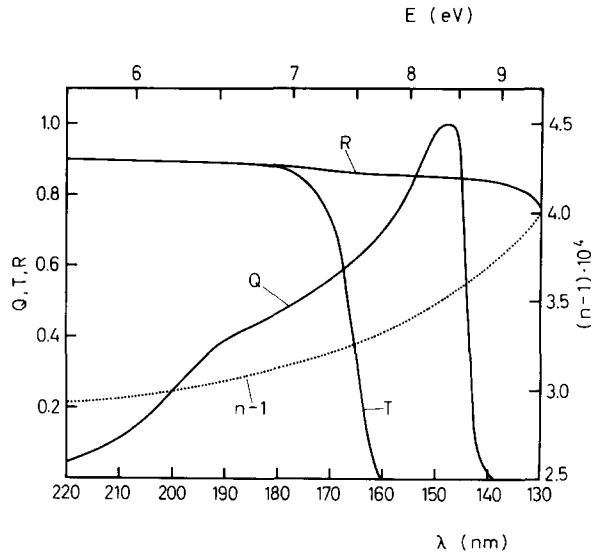

Fig. 3. Quantum efficiency $Q(\lambda)$ for TMAE, mirror reflectivity $R(\lambda)$ for a mirror with 800 Å Al and 380 Å MgF_2 coating [7], transmission $T(\lambda)$ of a 1.7 mm Suprasil window, and index of refraction (n-1) of N_2 at atmospheric pressure and 40°C.

To obtain a good spatial resolution a uniform electric field is needed. The electric field in the drift region is formed by a field cage which consists of 1.5 mm thick epoxy fibre glass, plated with copper strips 2 mm apart on both sides, and of the entrance window having 120 μm goldplated molybdenum wires on both sides in order to avoid polarization effects in the insulator. These wires are also 2 mm apart and reduce the transparency of the window by 10%.

The entrance window of the photon detector is made of quartz (Suprasil), 1.7 mm thick. The transmission $T(\lambda)$ is shown in fig. 3. Because of the cutoff at 160 nm we use tetrakis (dimethylamino) ethylene (TMAE) as the photosensitive gas which has a high quantum efficiency for wavelengths above 160 nm.

3. The gas supply system

As the vapor pressure of TMAE is low (0.4 Torr at room temperature [5]) one has to bubble the drift gas through warm TMAE. At 30°C the admixture of TMAE to the detector gas reduces the optical absorption length to 1.1 cm, so that the 5 cm thick drift region absorbs 99% of the Cherenkov photons. The necessity of using TMAE to match the transmission of the quartz window has two drawbacks. Firstly, the whole apparatus has to be kept at a temperature of 40°C to prevent the TMAE vapor from condensing on the detector parts. Secondly, the TMAE reacts with oxygen.

Fig. 4 shows the gas supply system which also was

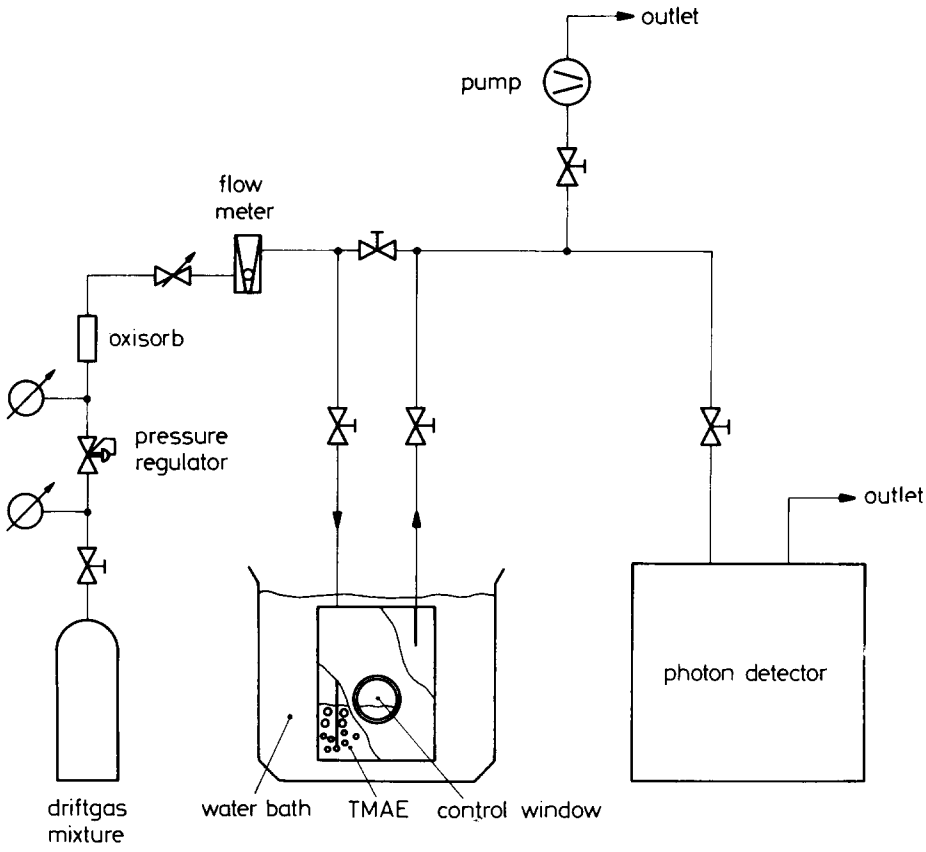

Fig. 4. Schematic view of the gas supply system.

used to purify crude or contaminated TMAE. All pipes and valves are made of stainless steel. They were kept at 40°C by electrical heating belts. The container for the TMAE was placed in a temperature controlled water bath which was set to a temperature of 30°C. The filling with TMAE was done by smashing a bottle of TMAE in the closed container. Before this procedure the container had been evacuated and filled with nitrogen. It turned out that this careful handling was not necessary and even exposing the TMAE to air was not harmful because in the following purification process the contaminated TMAE could be sufficiently purified. The purification of the TMAE was done by pumping on the filled container with a vacuum pump. The reaction products of the TMAE with oxygen and other impurities were boilded out and pumped away. After half an hour of pumping the TMAE was ready for use.

For the photon detector itself no special precautions were taken concerning the reaction of TMAE with the detector parts. The field cage including the voltage divider resistor chain was mounted inside a plastic box (PVC). The quartz window was glued with epoxy to the PVC. The wires were soldered to an epoxy fibreglass frame. During a period of one month no reactions of the TMAE with these materials were observed. In contrast, some materials which were used in an earlier test (silicon rubber, shrinking tubes, and a one component glue (Cyanacrylat)) showed a strong degradation when being exposed to a TMAE atmosphere: within half an hour a change in color was observed and a thin layer of TMAE or its decay products covered these parts of the detector. By avoiding such materials the photon detectors showed stable operating conditions over a four week running period during which the data were taken.

4. Test set-up and measurements

Fig. 5 shows the apparatus used in our measurements. The Cherenkov light was produced by 4 GeV/c electrons in a nitrogen radiator of 1.6 m length at atmospheric pressure. A spherical mirror of 1.22 m focal length focused the light onto the detector plane.

The mirror was made of a polished glass substrate with a 800 Å layer of aluminum covered with a 380 Å thick MgF_2 coating. The reflectivity $R(\lambda)$ is shown in fig. 3. In the working region of the photon detector, i.e. at photon energies below the cutoff of the quartz window

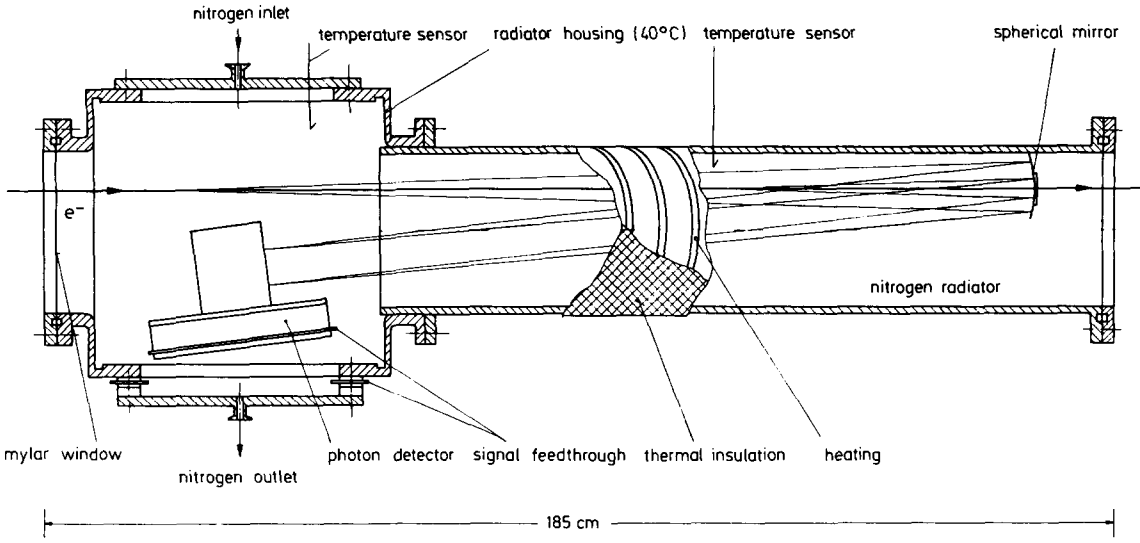

Fig. 5. Test Cherenkov counter with N_2 radiator, spherical mirror, and photon detector. Shown is the arrangement with the e^- test beam missing the photon detector.

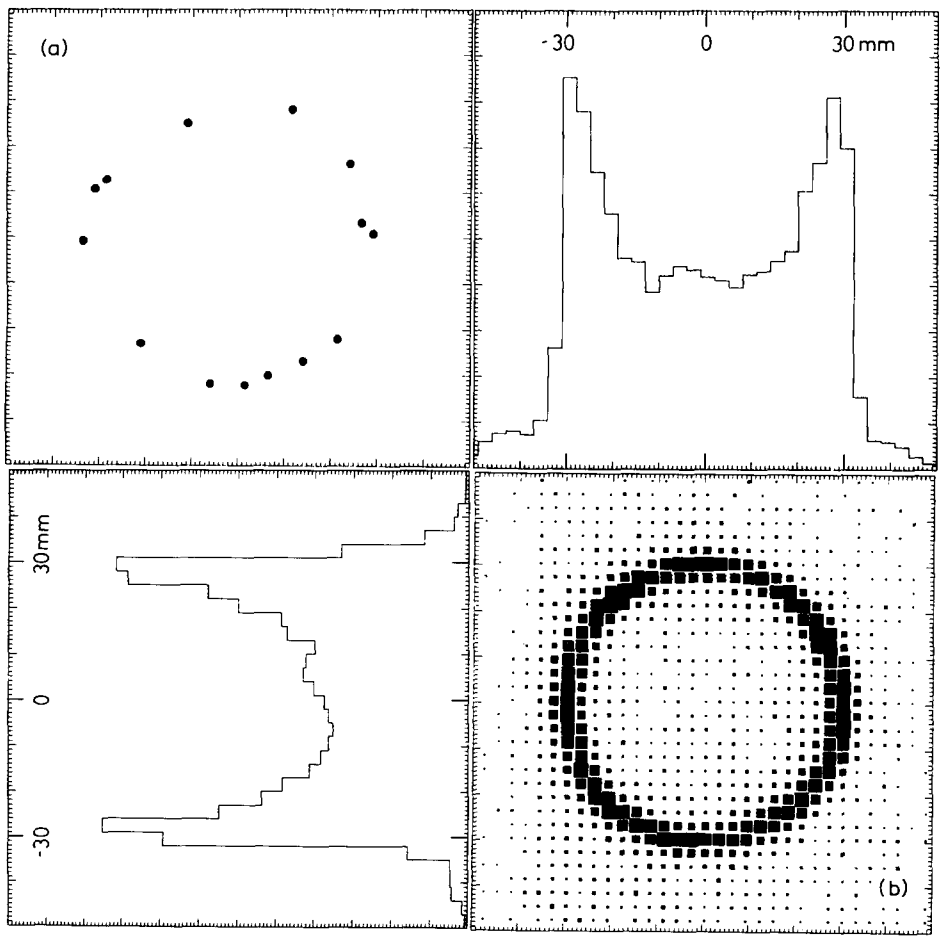

Fig. 6. (a) The conversion points of an event with 14 photoelectrons in a *xy* correlation plot. (b) *xy* correlation plot, with projections, summed over 2500 events.

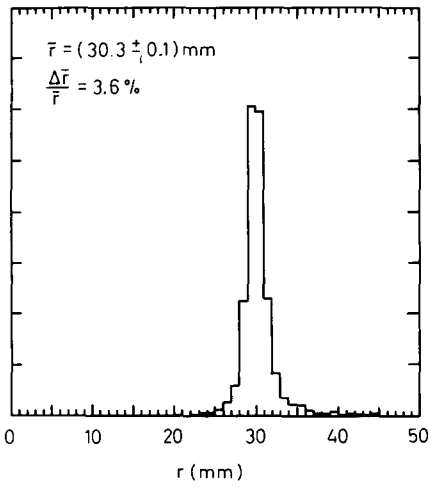

Fig. 7. The reconstructed radius of the Cherenkov ring image for 2500 events.

and above the threshold for photoionisation of the TMAE, the reflectivity is roughly constant with a value of 85%. The position of the mirror was adjustable, so that it was possible to perform measurements either with the electron beam missing the photon detector (as shown in fig. 5) or penetrating it.

Calculations by Barrelet et al. have shows that with a multiwire proportional chamber as described above the electronic threshold used in our experiment gas multiplication factors of 10^5 are needed [6]. At this high gas gain many photons are produced in the avalanche close to the signal wire. Some of them may travel a long distance until they get absorbed by TMAE molecules releasing electrons that produce secondary hits on neighboring wires. This problem is most severe if the incident charged particle traverses the photon detector. Minimum ionizing particles produce about 250 electrons in the photon detector gas which all drift to one or two signal wires. To study the effects of secondary photon conversion, a second test was performed in

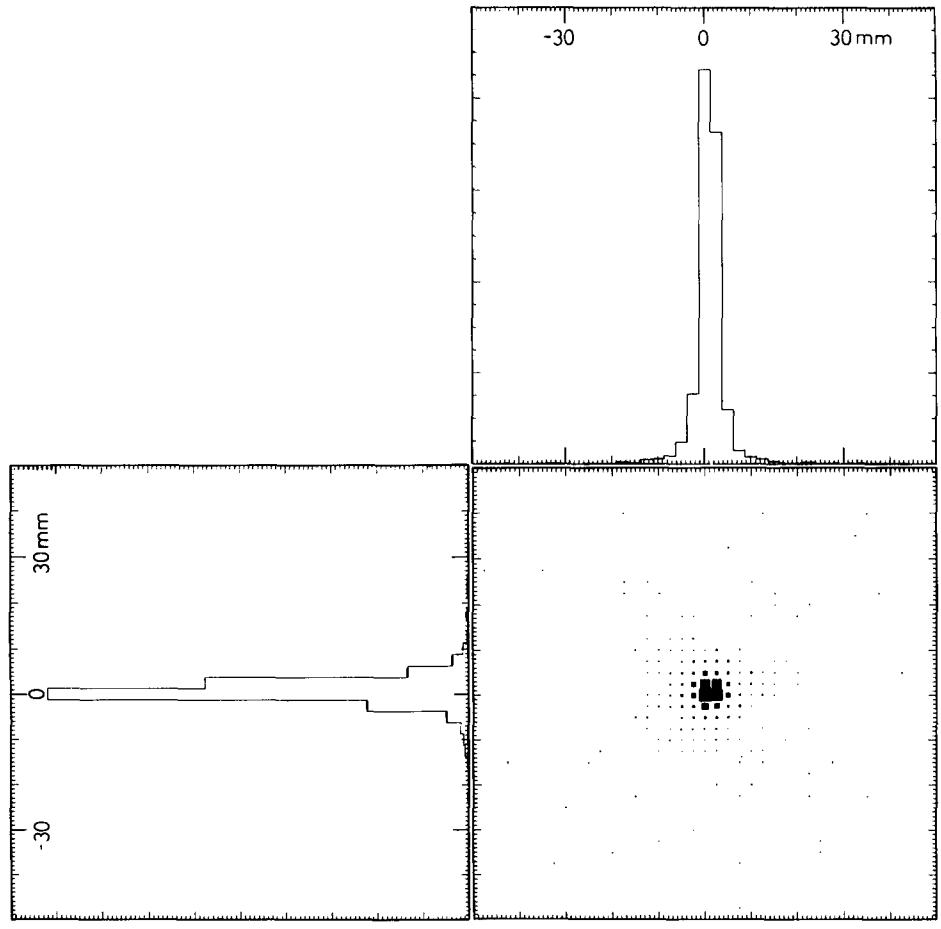

Fig. 8. *xy* correlation plot of the centres of the Cherenkov rings, with projections, summed over 2500 events.

which the signal wires were shielded from each other by separating walls.

4.1. Result on ring imaging

The measurements with unshielded signal wires and the incident particle beam missing the photon detector are summarized in figs. 6–12. Fig. 6a shows a particularly nice event with 14 photoelectrons on the Cherenkov ring. The superposition of 2500 triggers yields the Cherenkov ring image shown in fig. 6b together with the projections on the x and y axes. For each of these events a circle was fitted to the conversion points. Fig. 7 shows the distribution of the fitted radius r. The mean value of the radius is

$$\bar{r} = (30.3 \pm 0.1)\ \text{mm},$$

in good agreement with the expectation of $\bar{r} = 30.5$ mm from eq. (2). A correlation plot of the coordinates of the ring centres is given in fig. 8 together with the projections on the x and y axes. The width of the distributions is in agreement with the expectation from the 1 mrad divergence of the test beam.

To study the influence of the drift gas, three different mixtures were used: pure methane, 90% methane with 10% ethane, and 90% methane with 10% isobutane. The purities of the gases were 99% for methane and isobutane and 99.9% for ethane. The methane–ethane mixtures has a higher sensitivity than pure methane and yields an average of 9 photoelectrons per event. For the methane–isobutane mixture, the photoelectron yield is somewhat lower, because isobutane absorbs UV light below 170 nm and is therefore not so well matched to the transmission of the quarz window (see fig. 9).

Fig. 10a shows the measured average number of photoelectrons per trigger as a function of the high voltage applied to the signal wires. Fig. 10b shows the multiplicity distribution for the mixture methane–ethane at 3550 V, 100 V below the limit of stable operation. A Poisson distribution with $\bar{n} = 7.5$ describes the data quite well. For methane–isobutane, the average number of photoelectrons obtained from the Poisson fit is $\bar{n} = 6$ at 3600 V (fig. 10c). The numbers given above have to be corrected for background and for the loss of hits due to the use of single (last) hit TDC-electronics. The noise in the chamber and electronics was measured to contribute at most 0.5 photoelectrons. The background from secondary photon conversion depends strongly on the gas amplification.

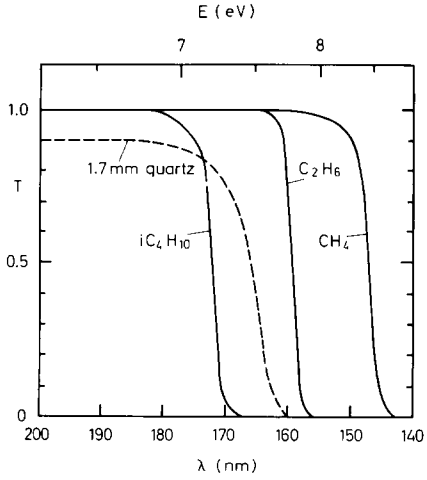

Fig. 9. Optical transmission of three different gas components and of the entrance window.

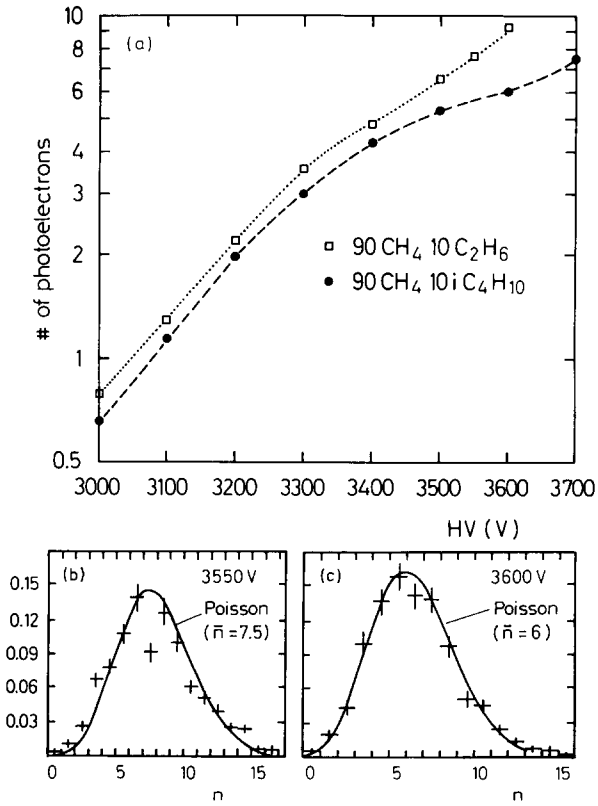

Fig. 10. (a) Measured number of photoelectrons per trigger versus the high voltage of the signal wires for two different gas mixtures. (b) Multiplicity distribution for 90% CH_4 10% C_2H_6. (c) Multiplicity distribution for 90% CH_4 10% iC_4H_{10}.

Conversions of secondary tend to occur close to the original avalanche. Thus, the absolute value Δy of the difference in the drift coordinate y between a hit and its neighbor tends to have smaller values for hits resulting from secondary photon conversion than for those belonging to the primary Cherenkov ring image. Fig. 11a shows the observed ring for an event with 14 hits. The ring is divided into the three regions A, B and C (wires no. 1–14, 15–24 and 25–40). To enhance the sensitivity in the measurement of Δy, only hits in the regions A

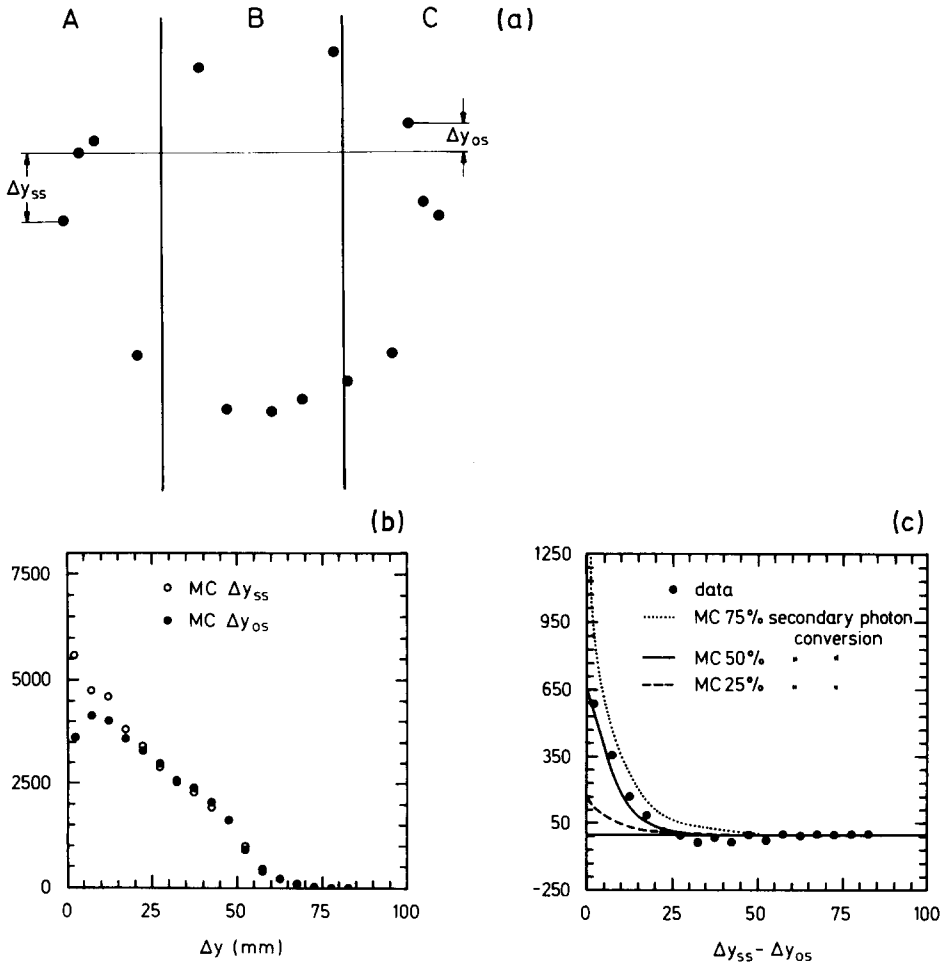

Fig. 11. (a) Definition of the regions A, B, and C and of the difference in y for two neighboring wires. (b) Difference in y for two neighboring wires for Monte Carlo events with 50% propability of emitting a secondary photon in the gas multiplication process. (c) Difference of the two curves Δy_{ss} and Δy_{os} for 90% CH_4 10% C_2H_6 compared with Monte Carlo events of different secondary photon emission propabilities.

and C, where Δy has on the average larger values than in the region B, were considered in the following.

To study the contributions from secondary photon conversion events were generated by a Monte Carlo method with the probability of an additional hit resulting from such conversions set to 50% per avalanche. The simulation also generated 0.5 random background hits per event and included the effect of our single hit electronics. Fig. 11b shows the distribution of the quantity Δy for the simulated events (1) for "same side" hits, i.e. both hits occurring in the same region (Δy_{ss}) and (2) for "opposite side" hits, i.e. one hit being in region A and the "neighboring" being in region C and vice versa (Δy_{os}). The difference of the two distributions reflects the effect of secondary photon conversions. In fig. 11c this difference is plotted for data taken with the methane–ethane gas mixture at a high voltage setting

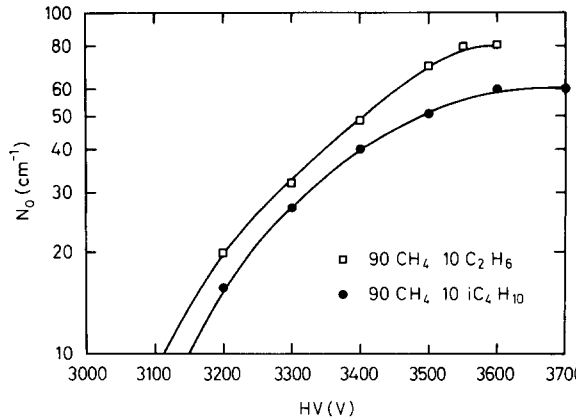

Fig. 12. Specific detector response for single hit electronic, electronic background, and secondary photon conversions as a function of the high voltage of the signal wires.

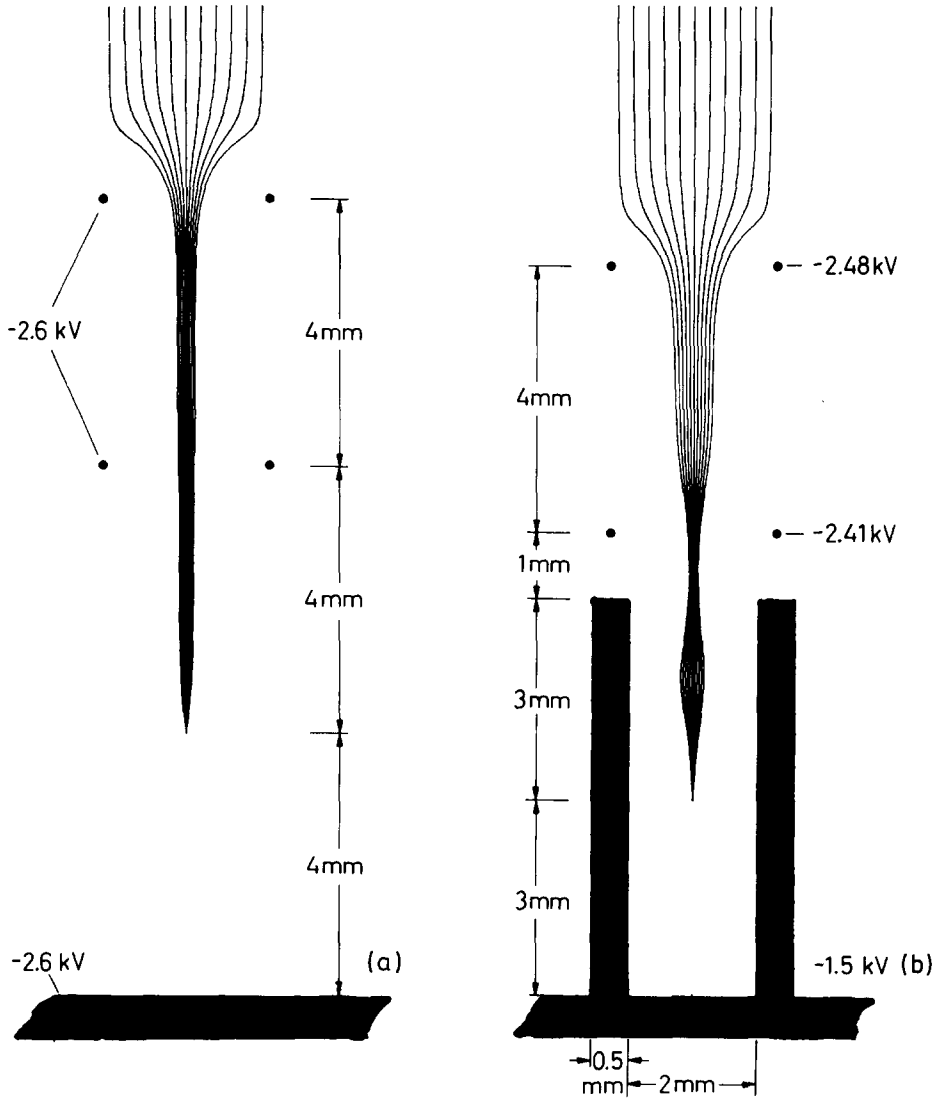

Fig. 13. Electric field lines for (a) unprotected signal wires and (b) shielded signal wires.

close to the limit of stable operation. The curves in fig. 11c are taken from the Monte Carlo generated events. The assumption of a 50% probability per avalanche for an additional hit to result from secondary photon conversion seems to describe the data well. Fig. 12 shows the specific detector response N_0 after correction of the data by the method described above.

4.2. Shielded signal wires

In order to reduce the probability of secondary photon conversion two methods can be employed: one can add quenching mixtures like ethane or isobutane and one can insert shielding walls between the signal wires thus absorbing most of the photons.

Fig. 13 shows the geometry and the field lines of the

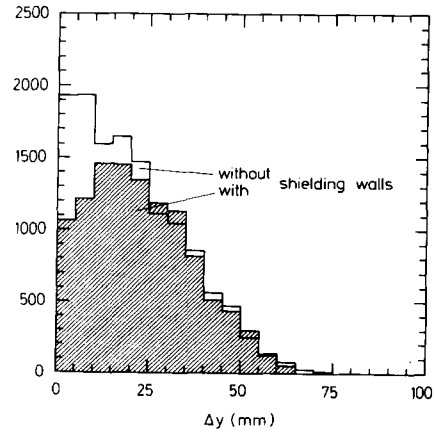

Fig. 14. Difference in y for two neighboring wires for CH_4.

configurations with and without shielding walls. Two layers of field guard wires were added to make sure that all the field lines coming from the drift region reach the signal wires and do not end at the shileding wall. The walls are made of graphite coated plastic.

The result of this modification is demonstrated in fig. 14 where Δy is plotted for methane at high voltage settings close to the limit of stable operation. The shaded curve shows that with shielding walls the amount of entries at small Δy is significantly reduced, i.e. due to the shielding walls no photons produced in the avalanche process can convert in the region close to neighboring wires.

We should note that with this type of chamber we obtained 5 photoelectrons per trigger. This might be due to a loss of fieldlines i.e. not all lines coming from the drift region reach the signal wire, in contrast with our two dimensional field calculations (see fig. 13).

The reduction of the photon induced crosstalk is not sufficient. Fig. 15 shows the xy correlation plot of events when the particles are penetrating the chamber. The high voltage had to be restricted to a value where only 1.5 Cherenkov photoelectrons were produced. Even at this low value the direct particle trajectory produced 4 hits.

5. Conclusions

We have tested successfully a ring imaging Cherenkov counter with time projection chamber type readout. The highest number of photoelectrons per event $N_{pe} = 8$ was obtained with a drift gas mixture of 90% methane with 10% ethane bubbling through 30°C warm TMAE. This number results in an electron yield of

$N_0 = 80\ \text{cm}^{-1}$.

This has to be compared to the theoretical value which is given by eq. (4) and results in $N_0 = 150\ \text{cm}^{-1}$. The resolution of the radius of the Cherenkov ring image

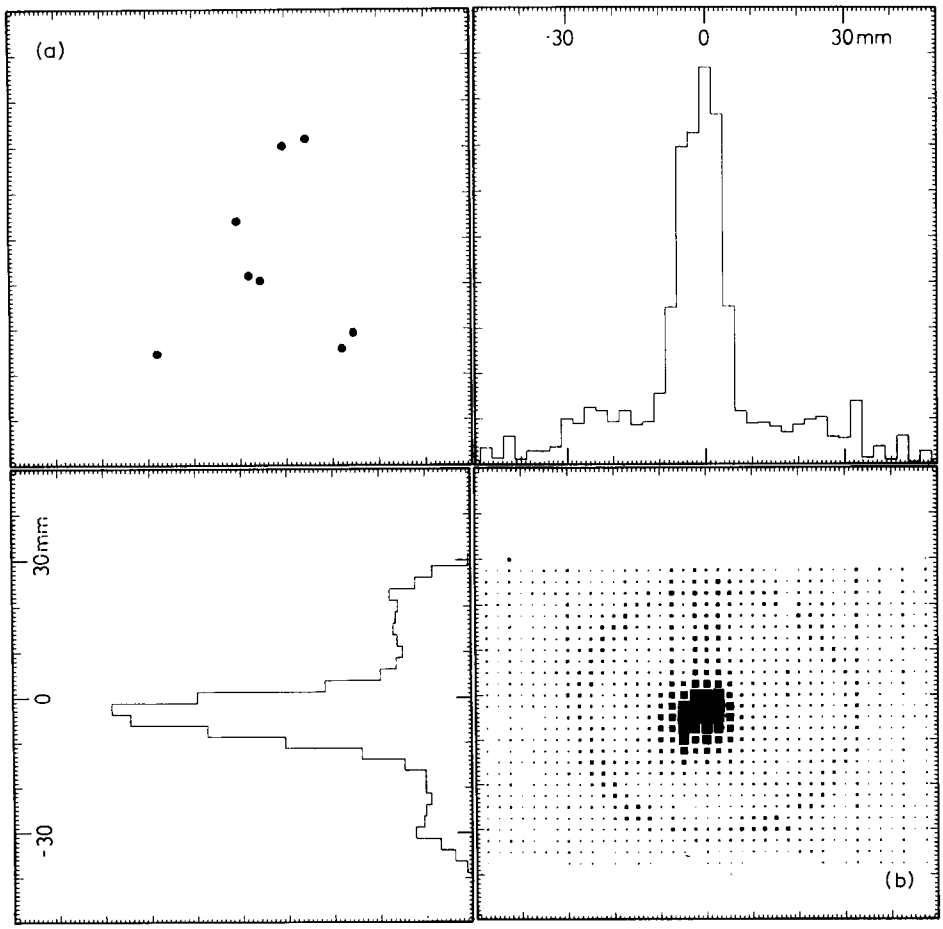

Fig. 15. (a) xy correlation plot of the conversion points and the electrons produced by the direct particle beam of one event. (b) xy correlation plot, with projections, summed over 2500 events.

was measured to be

$\Delta\bar{r}/\bar{r} = 3.6\%$.

The value of the measured error $\Delta\bar{r} = 1$ mm is in agreement with the estimated contributions from the various detector components which are: for the multiwire proportional chamber $\sigma_x = 0.72$ mm, for the drift region due to diffusion $\sigma_D = 0.5$ mm and drift time measurement $\sigma_y = 0.15$ mm, for chromaticity of n $\sigma_c = 0.5$ mm, and for optical errors $\sigma_0 = 0.5$ mm. The crosstalk from photons initiated in the avalanche process of neighboring wires was estimated to contribute up to 50% per hit. Adding shielding walls between the signal wires and using gases which match the quartz window reduces the background from this crosstalk significantly.

We would like to thank Prof. Dr. B.H. Wiik for his support and encouragement of this work. For the construction of the gas supply system we are very grateful to Dr. G. Poelz, C.-H. Sellmer and especially to D. Brauer who also helped us very much in setting up the test equipment. Thanks are due to H.-J. Schirrmacher for his help on the development of the preamplifiers and to Z. Zeiger for coating the mirror. We thank Prof. Dr. P. Schmüser and Dr. D. Pandoulas for their valuable remarks on this paper.

References

[1] A. Roberts, Nucl. Instr. and Meth. 9 (1960) 55.
[2] J. Séguinot and T. Ypsilantis, Nucl. Instr. and Meth. 142 (1977) 377.
[3] G. Coutrakon et al., Nucl. Instr. and Meth. 205 (1983) 403.
[4] E. Barrelet et al., Nucl. Instr. and Meth. 200 (1982) 219.
[5] D.F. Anderson, IEEE Nucl. Sci. Symp. (1980).
[6] E. Barrelet et al., Nucl. Instr. and Meth. 200 (1982) 219.
[7] P.H. Berning, G. Hass and R.P. Madden, J. Opt. Soc. Am. Meth. 50 (1960) 586.